Supporting online material for

Torque generation by axonemal outer-arm dynein

Shin Yamaguchi*, Kei Saito*, Miki Sutoh*, Takayuki Nishizaka†, Yoko Y. Toyoshima* and Junichiro Yajima*‡

*Department of Life Sciences, Graduate School of Arts & Sciences, The University of Tokyo, 3-8-1 Komaba Meguro-ku,Tokyo, 153-8902, Japan; †Department of physics, Gakushuin University, 1-5-1 Mejiro, Toshima-ku, Tokyo, 171-8588, Japan.
‡Correspondence should be addressed to J.Y. (yajima@bio.c.u-tokyo.ac.jp)

Supporting figure 1; Purification of outer-arm dynein and its subparticles from *Tetrahymena* ciliary axonemes.

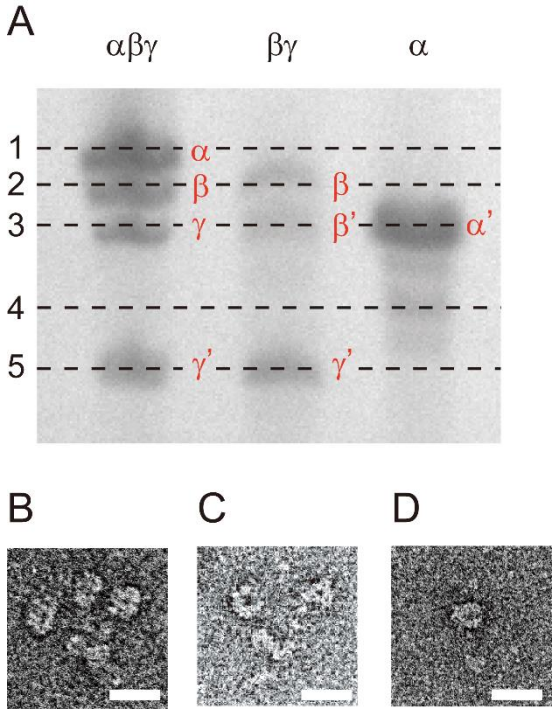

(*A*) SDS-urea-PAGE gel of purified outer-arm dynein and its subparticles. SDS-urea-PAGE was performed as described previously (1). Each dynein was loaded on a 3.2% polyacrylamide gel containing 6 M urea. Heavy chains comprising outer-arm dynein and its subparticles (α and βγ) were separated on the SDS-urea gel. Each band was numbered 1 to 5 and identified as heavy chain α, β or γ as described previously (1). α', β' and γ' mean the respective digested product of each heavy chain. (*B-D*) Negatively stained EM images of purified outer-arm dynein and its subparticles. 10 µl of purified dynein (about 20 nM) was applied to carbon coated copper grids and negatively stained with 1.5% (w/v) uranyl acetate. The specimens were examined in an electron microscope (Hitachi, H-7500) at an original magnification of 40,000× operating at 80 kV. The images show purified three-headed outer-arm dynein (*B*), two-headed βγ-subparticle (*C*) and one-headed α-subparticle (*D*). However, such a bouquet structure of three-headed outer arm dynein is different from the stacked form observed in axonemes (2)(3). Scale bar, 20 nm.

Supporting figure 2; Tracking uncertainty of 3D measurement.

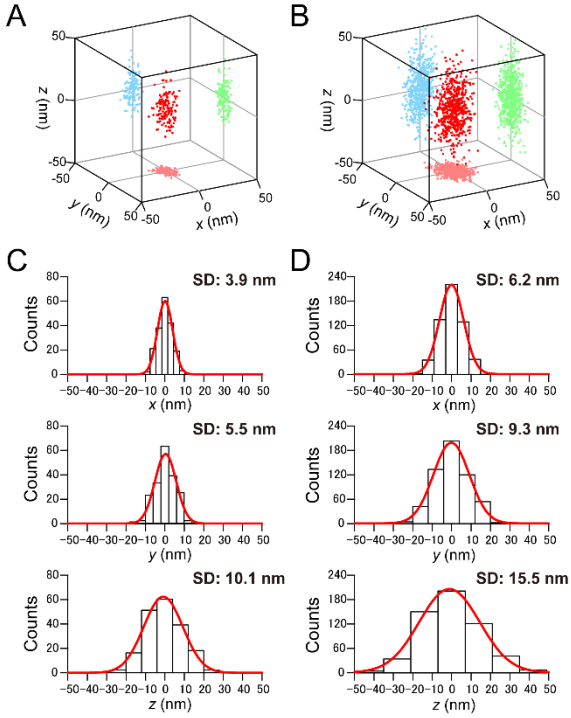

The 3D-plot shows positions of a QD attached to a microtubule fixed on a glass surface during 2 seconds at 10 frames per seconds (*A*) and 30 frames per seconds (*B*). Standard deviations (SDs) of *x*, *y* and *z* were derived from a Gaussian fitting (*C*, *D*).

Supporting figure 3; Rotational pitch of GMP-CPP microtubules.

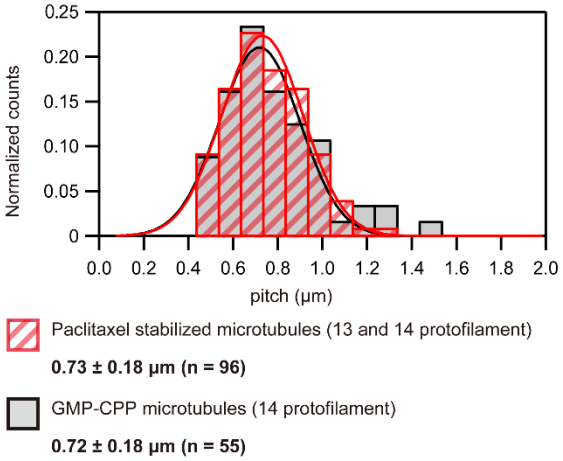

A histogram of rotational pitch of paclitaxel stabilized microtubules (red) and GMP-CPP microtubules (black) driven by αβγ at 10 µM ATP. The pitch of GMP-CPP microtubules had a similar distribution to that of paclitaxel stabilized microtubules (p = 0.52 in *t*-test). Curves represent Gaussian fits to the data, giving mean pitches of 0.73 ± 0.18 µm (mean ± SD, paclitaxel stabilized microtubules) and 0.72 ± 0.18 µm (mean ± SD, GMP-CPP microtubules), respectively.

Supporting figure 4; Relation of microtubule length to corkscrewing motion.

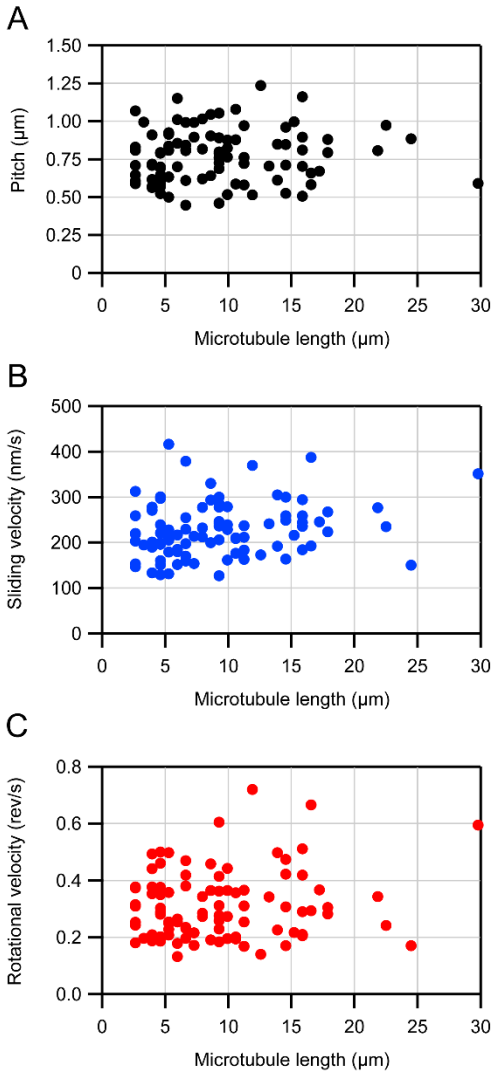

Pitch (*A*), sliding velocity (*B*) and rotational velocity (*C*) driven by αβγ at 10 µM ATP are plotted by microtubule length. Microtubule lengths were measured with the line tool of Image J (n = 90). Microtubules where the entire length was not within the field of view were rejected. Microtubule length was not correlated to the corkscrewing motion, as estimated by the Pearson correlation coefficient (R) between microtubule length and each data set. R = 0.08 (pitch), 0.22 (sliding velocity) and 0.15 (rotational velocity).

Supporting figure 5; Corkscrewing motion of a sliding microtubule driven by αβγ at 1 μM ATP and 100 μM ATP.

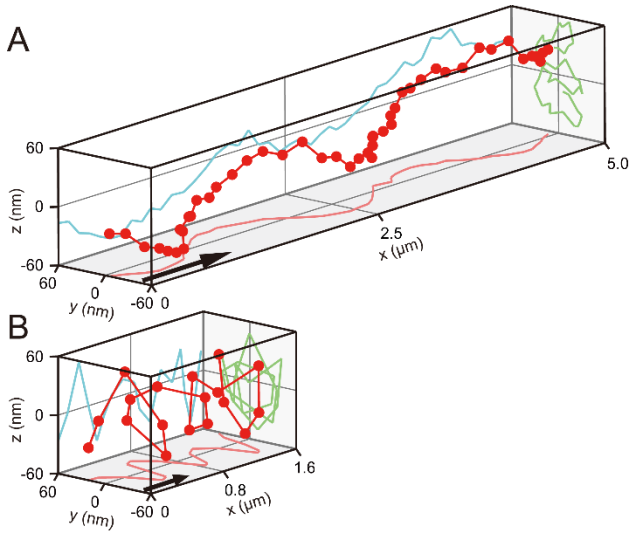

3D plot of a QD bound to a sliding microtubule driven by αβγ at 1 μM ATP (*A*) and 100 μM ATP (*B*). Images were either recorded at 2 s intervals and five images were averaged (*A*) or recorded at 0.1 s intervals with no averaging (*B*). The pitch value of corkscrewing motion is 2.0 μm (*A*) and 0.50 μm (*B*), respectively. In the presence of 1 or 100 μM ATP, αβγ is able to rotate microtubules in a clockwise manner, which is the same direction as observed in the presence of 10 μM ATP (**Fig. 1 *G***). The black arrows in (*A*) and (*B*) indicate displacement during 100 seconds (*A*) and 0.5 seconds (*B*), respectively.

Supporting figure 6; ATP concentration dependency of corkscrewing motion driven by an equimolar mixture of α and βγ.

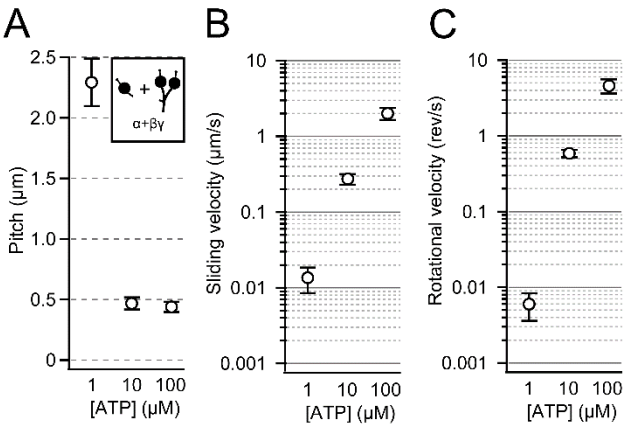

D

ATP	α + βγ		
concentration	pitch	sliding velocity	rotational velocity
μM	μm	μm/s	rev/s
1	2.3 ± 0.2 (5/9)	0.013 ± 0.005	0.006 ± 0.002
10	0.47 ± 0.05 (9/9)	0.27 ± 0.04	0.59 ± 0.7
100	0.44 ± 0.04 (35/36)	2.0 ± 0.4	4.6 ± 1.0

(*A*) Microtubule rotational pitches driven by a mixture of 0.4 μM α-subparticle and 0.4 μM βγ-subparticle are plotted at 1, 10 and 100 μM ATP. Data points and error bars indicate mean pitch and standard deviation, respectively. 0.4 μM βγ and 0.4 μM α were introduced into the experimental chamber once. Sliding velocity (*B*) and rotational velocity (*C*) are plotted against ATP concentration. (*D*) Summary of corkscrewing motion driven by the mixture at 1, 10 and 100 μM ATP. Of 54 sliding QD-attached microtubules, 49 rotated. The other 5 did not rotate. Values of denominator in parentheses are the number of microtubules analyzed and values of numerator are the number of microtubules rotated. Errors are standard deviations.

Supporting table 1; Summary of corkscrewing motion driven by the mixture at 1 μM ATP.

Parameter	Value for each assay					
α (μM)	0	0.1	0.3	0.4	0.8	1.5
βγ (μM)	0.8	0.7	0.5	0.4	0	0
Mole fraction of α	0	0.125	0.375	0.5	1	1
Pitch (μm)	0.8 ± 0.2	1.7 ± 0.3	1.8 ± 0.5	2.3 ± 0.2	1.7 ± 0.5	2.1 ± 0.3
Sliding velocity (μm/s)	0.035 ± 0.009	0.023 ± 0.004	0.012 ± 0.003	0.014 ± 0.005	0.008 ± 0.003	0.010 ± 0.002
Rotational velocity (rev/s)	0.049 ± 0.024	0.014 ± 0.004	0.007 ± 0.002	0.006 ± 0.002	0.005 ± 0.003	0.005 ± 0.001
Count of microtubules analyzed	27	9	7	9	5	12
Count of microtubules corkscrewed	19	8	5	5	4	9

Supporting movie 1

The movie shows a sliding rhodamine-labeled microtubule driven by αβγ for first ~2 seconds (0.2 s intervals, actual speed, G-2A filter set, Nikon), and a moving QD fixed to the microtubule via a streptavidin-biotin interaction for remaining ~15 seconds (0.2 s intervals, ×4 actual speed, QD 525 filter set, Chroma). Image, 18 μm high, 32 μm wide.

Supporting references

1. Toyoshima, Y.Y. 1987. Chymotryptic digestion of Tetrahymena ciliary dynein. II. Pathway of the degradation of 22S dynein heavy chains. J. Cell Biol. 105: 897–901.

2. Pigino, G., A. Maheshwari, K.H. Bui, C. Shingyoji, S. Kamimura, et al. 2012. Comparative structural analysis of eukaryotic flagella and cilia from Chlamydomonas, Tetrahymena, and sea urchins. J. Struct. Biol. 178: 199–206.

3. Maheshwari, A., and T. Ishikawa. 2012. Heterogeneity of dynein structure implies coordinated suppression of dynein motor activity in the axoneme. J. Struct. Biol. 179: 235–41.